

Assessing species interactions using integrated predator-prey models

Matthieu Paquet and Frédéric Barraquand

Institute of Mathematics of Bordeaux,
University of Bordeaux, CNRS, Bordeaux INP, Talence, France

Abstract

1
2 Inferring the strength of species interactions from demographic data is a challenging task. The
3 Integrated Population Modelling (IPM) approach, bringing together population counts, capture-
4 recapture, and individual-level fecundity data into a unified model framework, has been extended
5 from single species to the community level. This allows to specify IPMs for multiple species with
6 interactions specified as links between vital rates and stage-specific densities. However, there is no
7 evaluation of such models when interactions are actually absent—while any interaction inference
8 method runs the risk of producing false positives. We investigate here whether multispecies
9 IPMs could output interactions where there are in fact none, building on an existing predator-
10 prey IPM. We show that interspecific density-dependence estimates are centered on zero when
11 simulated to be zero, and therefore their estimation is unbiased. Their coverage probability,
12 quantifying how many times credible intervals include zero, is also satisfactory. We further
13 confirm that adding random temporal variation to multispecies density-dependent link functions
14 does not alter these results. An update of the observation model additionally shows that the data
15 requirements of the model could have been a little underestimated, as convergence is difficult to
16 reach for previously considered data scenarios. This study therefore reaffirms the potential of
17 multispecies IPMs to infer correctly how biotic interactions influence demography, although it
18 also shows that the data requirements of such models might have to be revised upwards.

19 **Keywords:** Integrated Population Model; data assimilation; species interactions; predation;
20 density-dependence.

21
22 Correspondence to matthieu.paquet@outlook.com, frederic.barraquand@u-bordeaux.fr

1 Introduction

As dynamic population models with interactions between species are data-hungry, with S^2 interaction parameters for S species, ecological statistics searches for improved ways to infer such population-level interaction strengths. A recently developed technique consists in combining data sources in multispecies Integrated Populations Models (IPMs) including those interspecific interactions (Péron & Koons, 2012; Barraquand & Gimenez, 2019; Quérroué *et al.*, 2021). Because Integrated Population Models (IPMs, Besbeas *et al.*, 2002) combine data on demographic rates (e.g., capture recapture, breeding data) with data on population size (typically from counts), they allow: (a) estimating both demographic rates and population size (and hence their inter-dependencies) in a joint analysis, (b) a improved precision in parameter estimates, compared to separate analyses of component datasets, since the information contained in several datasets combine into estimated parameters (e.g., count data and capture recapture data both contain information on survival rates), and in some cases (c) to estimate parameters for which there is no dedicated data stream, that can only be estimated through inverse estimation of a demographic model (Kéry & Schaub, 2011; Abadi *et al.*, 2010). This last property is particularly useful to estimate population-level species interactions strengths, since population-level interactions are indirectly inferred. Although inverse estimation can in theory be performed using a single data source such as population counts, such inverse estimation is a difficult task fraught with identifiability issues. Asking whether multispecies IPMs performed better than classical inverse estimation from count data alone, Barraquand & Gimenez (2019) have shown that better estimates of interaction parameters could be obtained by combining data sources. Additionally, Quérroué *et al.* (2021) have revealed which interactions were strong enough to be detected in an empirical bird predator-prey system, where bottom-up demographic linkages from prey to predator were found but top-down links were not, in spite of known predation and probable impacts on prey dynamics—top-down effects were likely too weak to be detected.

In these multispecies IPM studies estimating interspecific interactions, between-species linkages have always been considered to be present in the simulations or in the underlying reality (based on background knowledge). Other choices are possible: some multispecies IPMs do not assume interspecific interactions to be present a priori (Lahoz-Monfort *et al.*, 2017), but they do not estimate them either and focus instead on environmental effects. However, multispecies IPMs with interspecific interactions could also be used in situations where it is not clear whether population-level

54 interactions between species are possible. This is all the more true that interactions are specified as
55 links between vital rates and stage-specific densities, and while some of these relationships may be
56 known a priori, others may not. The issue was raised but not tackled by [Barraquand & Gimenez](#)
57 (2019): a natural follow-up is therefore to ask what happens whenever we try to estimate interac-
58 tions that are actually absent, to make sure that multispecies IPMs do not yield false positives.

59 Let us note that when estimating or predicting interspecific interactions in general—not just
60 with multispecies IPMs—whether methods could output false positives is a key concern (e.g., with
61 multivariate autoregressive models, [Barraquand et al. 2021](#); dynamic bayesian networks, [Sander](#)
62 [et al. 2017](#); or other machine learning tools, [Strydom et al. 2021](#)). The fact that all interaction
63 inference methods run the risk of creating false positives of interspecific interactions at exaggerated
64 rates only reinforces the need to evaluate it in multispecies IPMs.

65 An additional concern is temporal stochasticity in the functions linking vital rates of a given
66 stage of species i to the densities of another stage of species j . In the simulation-based study of
67 [Barraquand & Gimenez \(2019\)](#), it was assumed that such stochasticity was absent, while empirical
68 studies ([Péron & Koons, 2012](#); [Quéroué et al., 2021](#)) assumed its presence in order to partition
69 variation in vital rates due to species densities vs other factors changing over time. We therefore
70 still need to understand whether theoretical performances hold in this more empirically realistic
71 context, where environmental factors can perturb demographic rates, and those are not solely
72 deterministic functions of species densities.

73 To sum up, we follow-up here on the multispecies IPM study of [Barraquand & Gimenez \(2019\)](#)
74 by asking whether (1) inter-species interactions are truly estimated to be zero when species have
75 in fact independent dynamics and (2) how species interaction strengths estimates can be affected
76 by the absence and presence of environmental stochasticity (random year effects on demographic
77 rates).

78 **2 Methods**

79 **2.1 General description of the multispecies IPM**

80 We used the same predator-prey model structure and parameter values as [Barraquand & Gimenez](#)
81 (2019). The deterministic skeleton can be described as a density-dependent matrix population
82 model

$$\mathbf{n}_{t+1} = \mathbf{A}(\mathbf{n}_t)\mathbf{n}_t. \tag{1}$$

Eq. 1 describes in discrete-time the dynamics of abundances of two species and two stages per species, with projection matrix

$$\mathbf{A}(\mathbf{n}_t) = \begin{pmatrix} 0 & \frac{1}{2}f_{V,t} \left(n_{V,t}^A \right) \phi_{V,t}^J \left(n_{P,t}^A \right) & 0 & 0 \\ \phi_{V,t}^A & \phi_{V,t}^A & 0 & 0 \\ 0 & 0 & 0 & \frac{1}{2}f_{P,t} \left(n_{V,t}^J \right) \phi_{P,t}^J \left(n_{P,t}^A \right) \\ 0 & 0 & \phi_{P,t}^A & \phi_{P,t}^A \end{pmatrix}$$

and abundance vector

$$\mathbf{n}_t = \begin{pmatrix} n_{V,t}^J \\ n_{V,t}^A \\ n_{P,t}^J \\ n_{P,t}^A \end{pmatrix}$$

83 where $n_{V,t}^J, n_{V,t}^A, n_{P,t}^J$ and $n_{P,t}^A$ are respectively the abundances of juvenile prey (denoted V as 'vic-
84 tim'), adult prey, juvenile predators and adult predators, at time t . The fecundities $f_{V,t}, f_{P,t}$ are the
85 expected number of juvenile prey and predator produced by an adult prey and predator, respec-
86 tively. Survival probabilities between t and $t + 1$ are denoted with ϕ , so that $\phi_{V,t}^J, \phi_{V,t}^A, \phi_{P,t}^J$ and $\phi_{P,t}^A$
87 are the survival probabilities of the juvenile prey, adult prey, juvenile predator and adult predator.

88 2.1.1 Count data

89 To simulate and account for demographic stochasticity, we modelled yearly (st)age specific abun-
90 dances \mathbf{n}_t using Binomial and Poisson distributions as in Barraquand & Gimenez (2019) eqs. (2)–(5).

91 Regarding the observation process for count data, the 2019 model assumed a negligible obser-
92 vation error ($\sigma^2 = 10^{-5}$). The reason was that in absence of replicated counts at each time unit,
93 observation error variance is notoriously difficult to disentangle from process error variance (Knappe,
94 2008; Auger-Méthé *et al.*, 2016). While in some cases it could be possible to remove observation error
95 altogether, because total population sizes of each species (summed numbers of juveniles and adults)
96 are the observed count variables (as in most IPMs), they need to appear in the model as drawn from
97 some probability distribution—they need to be a stochastic node in the MCMC representation. It
98 was therefore decided to keep the formulation of the model in its state-space version, but forcing it
99 to observe true population size almost with certainty (negligible process error variance). However,
100 we uncovered in the present work that stage-specific abundances could not be estimated properly.

101 Because correctly reproducing stage-specific abundances when fitting a stage-structured model is
 102 desirable, and that there is in most wildlife surveys some measure of observation error on counts,
 103 we assumed in the present article a non-negligible, positive observation error variance. As we do
 104 not have replicated counts at any given time, we do not attempt to estimate observation error vari-
 105 ance, and assume that it is known and classically set on the logarithmic scale (i.e., the coefficient
 106 of variation of observed population size is constant). For predator counts (denoted P) we have:

$$y_{P,t} | \mathbf{n}_t \sim \mathcal{LN}(\log(n_{P,t}^J + n_{P,t}^A), \sigma_{obs}^2) \quad (2)$$

107 And similarly for prey counts :

$$y_{V,t} | \mathbf{n}_t \sim \mathcal{LN}(\log(n_{V,t}^J + n_{V,t}^A), \sigma_{obs}^2) \quad (3)$$

108 with \mathcal{LN} the log-Normal distribution and its associated variance on the log-scale $\sigma_{obs}^2 = 0.1$.

109

110 2.1.2 Survival data

111 To increase computational efficiency (particularly true for the scenarios with more individuals cap-
 112 tured and a shorter time series) compared to the 2019 model, we simulated and fitted the capture-
 113 mark-recapture data in the m-array format, using a multinomial likelihood (e.g., [Burnham, 1987](#)).
 114 The data is in the form of a $(T - 1) \times T$ matrix $\mathbf{M} = (m_{t,j})$, with $m_{t,j} = 0, \forall j < t$, where T is the
 115 total number of years of capture recapture history. $m_{t,t}$ is the number of individuals first marked
 116 as young at time t that were re-sighted the following year, and the last column $m_{t,T}$ is the number
 117 of individuals first marked at time t that were never re sighted. We then have:

$$\mathbf{m}_{t,\bullet} = (m_{t,t}, m_{t,t+1}, \dots, m_{t,T}) \sim \text{Multinomial}(N_t, (\theta_{t,t}, \dots, \theta_{t,T})) \quad (4)$$

118 with N_t the number of individuals first marked as young at time t .

119

120 Diagonal elements of the θ matrix write

$$\theta_{t,t} = \phi_t^J p$$

121 and for $t < j < T$

$$\theta_{t,j} = \phi_t^J \prod_{k=t+1}^j \phi_k^A (1-p)^{j-t} p.$$

122 The last element pertains to individuals never recaptured

$$\theta_{t,T} = 1 - \sum_{k=t}^{T-1} \theta_{t,k}.$$

123 Parameters ϕ_t^J and ϕ_t^A are respectively the first year and adult survival probabilities from year
124 t to year $t + 1$ (for the species considered), and p the recapture (or re-sighting) probability set as
125 constant among years and age classes.

126 Similarly, we also simulated and fitted m-array data of individuals first marked as adults $\mathbf{M}_a =$
127 $(m_{t,j}^{(a)})$ for which the above mentioned equations are identical to the exception that ϕ^J is replaced
128 by ϕ^A .

129 **2.1.3 Fecundity data**

130 Fecundity was modelled using a Poisson regression:

$$F_t \sim \text{Poisson}(f_t R_t) \tag{5}$$

131 with F_t the total number of offspring counted, R_t the number of surveyed broods/litters, and f_t the
132 expected fecundity per adult each year t .

133 **2.2 Alternative scenarios and parameter values**

134 **2.2.1 Density dependence and random temporal variation on demographic rates**

Intra- and inter-species density dependence of survival rates $\phi_{i,t}^j$ (with $i \in \{V, P\}$ and $j \in \{J, A\}$)
and fecundities $f_{i,t}$ were modelled on the logit and log scale, respectively, as in [Barraquand &](#)

Gimenez (2019). We initially used the same equations as the 2019 model, which are:

$$\text{logit}(\phi_{P,t}^J) = \alpha_1 + \alpha_2 n_{P,t}^A \quad (6)$$

$$\text{logit}(\phi_{V,t}^J) = \alpha_3 + \alpha_4 n_{P,t}^A \quad (7)$$

$$\text{logit}(\phi_{P,t}^A) = \alpha_{\phi_P^A} \quad (8)$$

$$\text{logit}(\phi_{V,t}^A) = \alpha_{\phi_V^A} \quad (9)$$

$$\log(f_{P,t}) = \alpha_5 + \alpha_6 n_{V,t}^J \quad (10)$$

$$\log(f_{V,t}) = \alpha_7 + \alpha_8 n_{V,t}^A \quad (11)$$

(see associated results in Supplementary Information Table S1 and Figures S5 to S8).

However, to limit posterior correlation between intercept and slope parameters and improve their estimation, we centered the abundances in the density dependent functions. While centering is typically done and most efficient on mean values, mean abundances varied here from a simulation to the next due to stochasticity. Therefore, intercept parameter values would have to be redefined for each simulation to maintain equivalent mean demographic rate values and asymptotic stage specific abundance equilibria for all simulation. To avoid these complications, we centered by subtracting the corresponding fixed point equilibria estimated in Barraquand & Gimenez (2019) as $\bar{n}_P^A = 21$, $\bar{n}_V^J = 101$ and $\bar{n}_V^A = 152$. The new α intercept parameters obey the following centered formulas:

$$\text{logit}(\phi_{P,t}^J) = \alpha_1 + \alpha_2 (n_{P,t}^A - \bar{n}_P^A) \quad (12)$$

$$\text{logit}(\phi_{V,t}^J) = \alpha_3 + \alpha_4 (n_{P,t}^A - \bar{n}_P^A) \quad (13)$$

$$\text{logit}(\phi_{P,t}^A) = \alpha_{\phi_P^A} \quad (14)$$

$$\text{logit}(\phi_{V,t}^A) = \alpha_{\phi_V^A} \quad (15)$$

$$\log(f_{P,t}) = \alpha_5 + \alpha_6 (n_{V,t}^J - \bar{n}_V^J) \quad (16)$$

$$\log(f_{V,t}) = \alpha_7 + \alpha_8 (n_{V,t}^A - \bar{n}_V^A). \quad (17)$$

To maintain equivalent dynamics to parameter set 1 of the 2019 model, we calculated the intercepts α_1 , α_3 , α_5 and α_7 as their original values plus the original slope multiplied by the estimated fixed point equilibrium of the n responsible for density dependence. For example, we now use whenever simulating $\alpha_3 = 0.5 - 0.025 \times 21 = -0.025$ and $\alpha_5 = 0 + 0.004 \times 101 = 0.404$ (Table 1).

148 In addition, we introduced scenarios with inter-annual random variation in the intercepts of
 149 density-dependent links, such that

$$\text{logit}(\phi_{P,t}^J) = \alpha_1 + \alpha_2(n_{P,t}^A - \bar{n}_P^A) + \sigma_{\phi_P^J} \epsilon_{\phi_P^J} \quad (18)$$

$$\text{logit}(\phi_{V,t}^J) = \alpha_3 + \alpha_4(n_{P,t}^A - \bar{n}_P^A) + \sigma_{\phi_V^J} \epsilon_{\phi_V^J} \quad (19)$$

$$\text{logit}(\phi_{P,t}^A) = \alpha_{\phi_P^A} + \sigma_{\phi_P^A} \epsilon_{\phi_P^A} \quad (20)$$

$$\text{logit}(\phi_{V,t}^A) = \alpha_{\phi_V^A} + \sigma_{\phi_V^A} \epsilon_{\phi_V^A} \quad (21)$$

with $\epsilon \sim \mathcal{N}(0, 1)$ i.i.d. and

$$\log(f_{P,t}) \sim \mathcal{N}(\alpha_5 + \alpha_6(n_{V,t}^J - \bar{n}_V^J), \sigma_{f_P}^2) \quad (22)$$

$$\log(f_{V,t}) \sim \mathcal{N}(\alpha_7 + \alpha_8(n_{V,t}^A - \bar{n}_V^A), \sigma_{f_V}^2). \quad (23)$$

150 Although mathematically identical, we used a parameterisation of the form $\mu + \epsilon\sigma$, $\epsilon \sim \mathcal{N}(0, \sigma^2)$
 151 (sometimes called non-centered) for survival estimates and a centered parameterisation ($\mathcal{N}(\mu, \sigma^2)$)
 152 for fecundity estimates as it was found to be optimal for the mixing of the MCMC chains. As we
 153 were primarily interested in the ability of multispecies IPMs to estimate species interactions when
 154 these were in fact absent, inter species density dependence parameter values for α_2 and α_4 were
 155 either set to zero for the simulations, or at the same value as in [Barraquand & Gimenez \(2019\)](#).
 156 Parameter values used to simulate data and their interpretation can be found in [Table 1](#).

157 2.2.2 Initial values and monitoring setup

For all simulation scenarios we used the initial population size vector

$$\begin{pmatrix} n_{V,1}^J \\ n_{V,1}^A \\ n_{P,1}^J \\ n_{P,1}^A \end{pmatrix} = \begin{pmatrix} 100 \\ 100 \\ 20 \\ 20 \end{pmatrix}$$

158 and the yearly number of monitored prey and predator broods/litters respectively $R_t^V = 50$ and
 159 $R_t^P = 20$. For consistency with [Barraquand & Gimenez \(2019\)](#), all scenarios were crossed with two
 160 alternative population monitoring duration and number of marked juveniles: either 100 juveniles

Table 1: Model parameters with their values. Values of α_4 and α_6 in the scenarios with true presence of species interactions are presented in brackets. Temporal standard deviations (SD) are only present in the scenarios with random temporal variation. For interpretation, note that α_i and temporal SD parameters are within exponential functions. For instance, $\alpha_5 = 0.404$ corresponds to a mean fecundity of $e^{0.404} \approx 1.5$.

Parameter	Value	Interpretation
α_1	0.29	juvenile predator survival – intercept
α_2	-0.01	juvenile predator survival – slope
α_3	-0.025	juvenile prey survival – intercept
α_4	0 (-0.025)	juvenile prey survival – slope – inter species density dependence
α_5	0.404	predator fecundity – intercept
α_6	0 (0.004)	predator fecundity – slope – inter species density dependence
α_7	1.24	prey fecundity – intercept
α_8	-0.005	prey fecundity – slope
p	0.7	recapture probability
$\alpha_{\phi_P^A}$	logit(0.7)	adult predator survival – intercept
$\alpha_{\phi_V^A}$	logit(0.6)	adult prey survival – intercept
σ_{obs}^2	0.1	observation error
σ_{f_P}	0.1	temporal SD of predator fecundity
σ_{f_V}	0.1	temporal SD of prey fecundity
$\sigma_{\phi_P^J}$	0.1	temporal SD of juvenile predator survival
$\sigma_{\phi_P^A}$	0.1	temporal SD deviation of adult predator survival
$\sigma_{\phi_V^J}$	0.1	temporal SD deviation of juvenile prey survival
$\sigma_{\phi_V^A}$	0.1	temporal SD deviation of adult prey survival

161 are marked each year for $T = 10$ years, or 20 juveniles are marked each year for $T = 30$ years,
162 for both species. However, due to the inclusion of non-negligible observation error in the counts,
163 our model faces convergence/practical identifiability issues for 29–56% of simulated data-sets at
164 these sample sizes (Figures S5 to S8). Therefore, we focus mostly in the present work on a new
165 scenario for which 100 juveniles are marked each year (we assume only juveniles are marked) for 30
166 years. Results using the previous monitoring setups (and the non centered density-dependencies)
167 are presented in the Supplementary Information B.

168 We consider two alternative situations without interspecific interactions, i.e., with or without
169 random temporal noise. To compare model performances in the no-interactions setting to cases with
170 interspecific interactions, we also simulated and fitted data in presence of species interactions using
171 the same α_i values as Barraquand & Gimenez (2019) under the four above-mentioned scenarios (i.e.,
172 with/without interactions \times with/without stochasticity on interactions; see Supplementary Table 2
173 and Figures S1 and S3). For each of these four combinations of parameter sets, we simulated 100
174 datasets using the Nimble package (de Valpine *et al.*, 2017, 2022, version 0.12.2) in R (R Core Team,
175 2022, version 4.2.1).

176 2.3 Priors specification and model fitting

177 Multispecies IPMs were implemented in a Bayesian framework, hence the need to specify priors.
178 When fitting the models to simulated data, we used $\mathcal{N}(100, 10)$ and $\mathcal{N}(20, 10)$ priors for the initial
179 stage-specific prey and predator population sizes (truncated to be positive). These priors also
180 differed from Barraquand & Gimenez (2019) where they were all set to $\mathcal{N}(25, 10^{-5})$.

181 Priors for standard deviations were chosen as $\sigma \sim \text{Exp}(1)$, which corresponds to priors with max-
182 imum entropy on the log and logit scales (e.g., McElreath, 2020). Prior probabilities of recapture
183 were drawn as $p \sim \text{Unif}(0, 1)$ and vital rate/interaction parameters were given weakly informative
184 priors $\alpha_k \sim \mathcal{N}(0, 1)$ ($k \in 1, \dots, 8$).

185 Data were both simulated and fitted using the Nimble R package (R Core Team, 2022; de
186 Valpine *et al.*, 2017, 2022, version 0.12.2). To improve their mixing and minimize their posterior
187 correlations, intercepts, slopes and temporal SD were block sampled using automated factor slice
188 samplers (Tibbitts *et al.*, 2014; Ponisio *et al.*, 2020). For each simulated dataset, we fitted the same
189 multispecies IPM that was used to generate the data (e.g., no random temporal noise estimated on
190 data without temporal noise), except in that species interactions were estimated even in absence of
191 such interactions. Two MCMC chains were run for 40000 iterations and we sampled the last 20000

192 iterations every 20th iteration leading to 2000 posterior samples saved per dataset. Real parameter
193 values were used as initial values to minimise time to convergence (see Appendix Section C for
194 an evaluation of the influence of initial values on parameter estimation). We assess convergence
195 and mixing of the chains for all α_i by calculating the potential scale reduction factor (\hat{R} , Brooks &
196 Gelman 1998; Gelman & Rubin 1992) and effective sample size ($n_{eff.}$) using the "gelman.diag()" and
197 the "effectiveSize()" functions of the *coda* package (Plummer *et al.*, 2006, version 0.19-4). We only
198 used outputs from models for which all α_i had $\hat{R} < 1.1$ and $n_{eff.} > 50$, that is, 96/100 models for
199 the scenario without random temporal variation and 73/100 models for the scenario with random
200 temporal variation. The computer code is provided at [https://github.com/MatthieuPaquet/](https://github.com/MatthieuPaquet/multi_species)
201 [multi_species](https://github.com/MatthieuPaquet/multi_species).

202 **3 Results**

203 Overall, the estimation of density dependence curves did not show any sign of bias for interspecific
204 density dependence (either absent, Figures 1 and 3 or present, Figures S1 and S3) and intraspecific
205 density dependence. This was true without and with temporal stochasticity (Figures 1 to 4).

206 This absence of bias extends to the alternative data designs with smaller sample sizes considered
207 in Barraquand & Gimenez (2019) (shown in Supplementary Information in Figures S5 to S8).
208 Estimated α_i parameters also did not show sign of bias in any scenario (Tables S1 and 2).

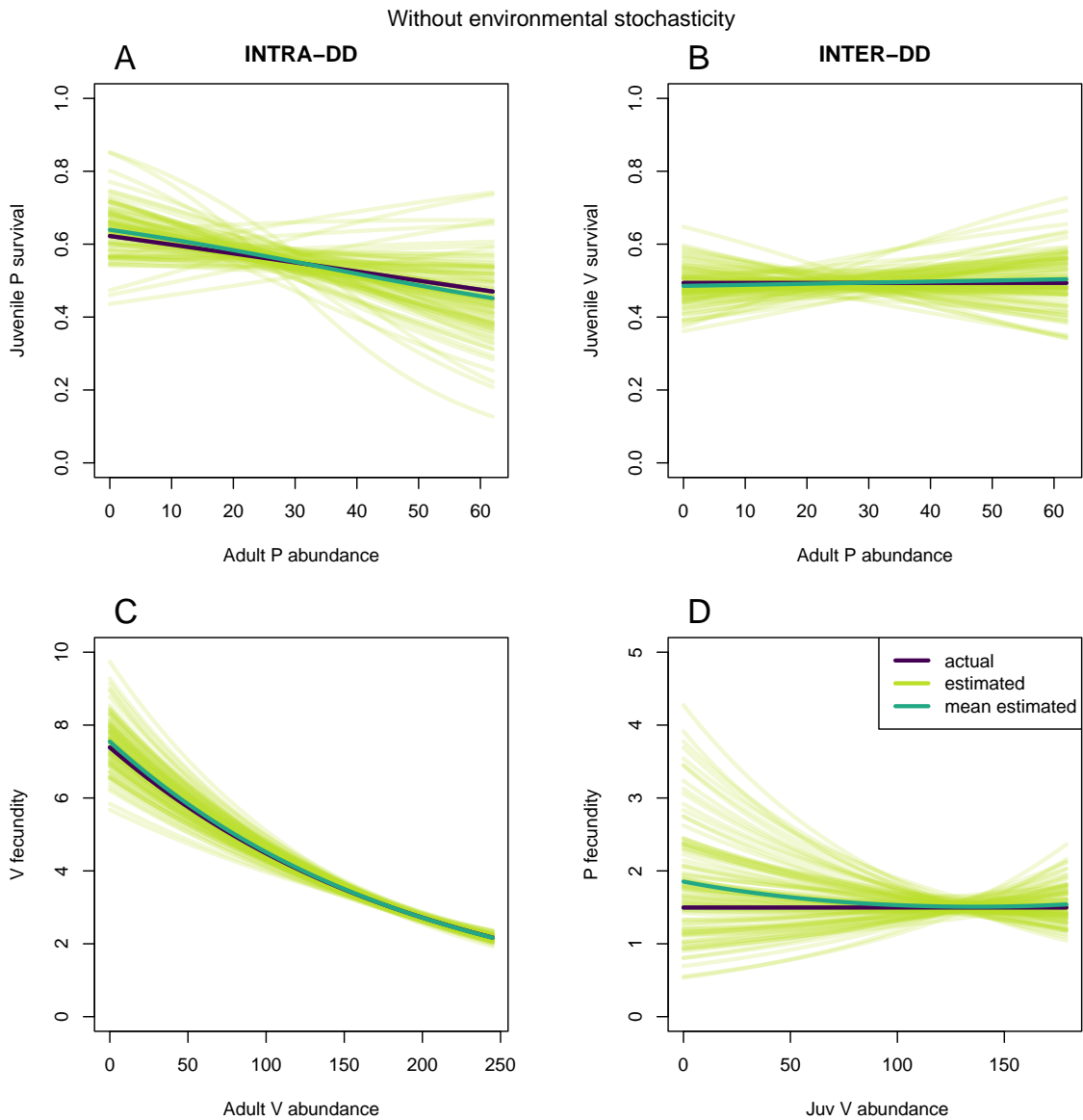


Figure 1: Density-dependencies for juvenile survival rates (**A** for predator and **B** for prey) as well as prey (**C**) and predator (**D**) fecundities in the scenario without random time variation. Purple: simulated relationships, light green: posterior mean relationships for the 96 fitted models that appear to converge satisfactorily, dark green: average of the posterior mean relationships. True inter species density-dependencies (right panels) were set to be absent.

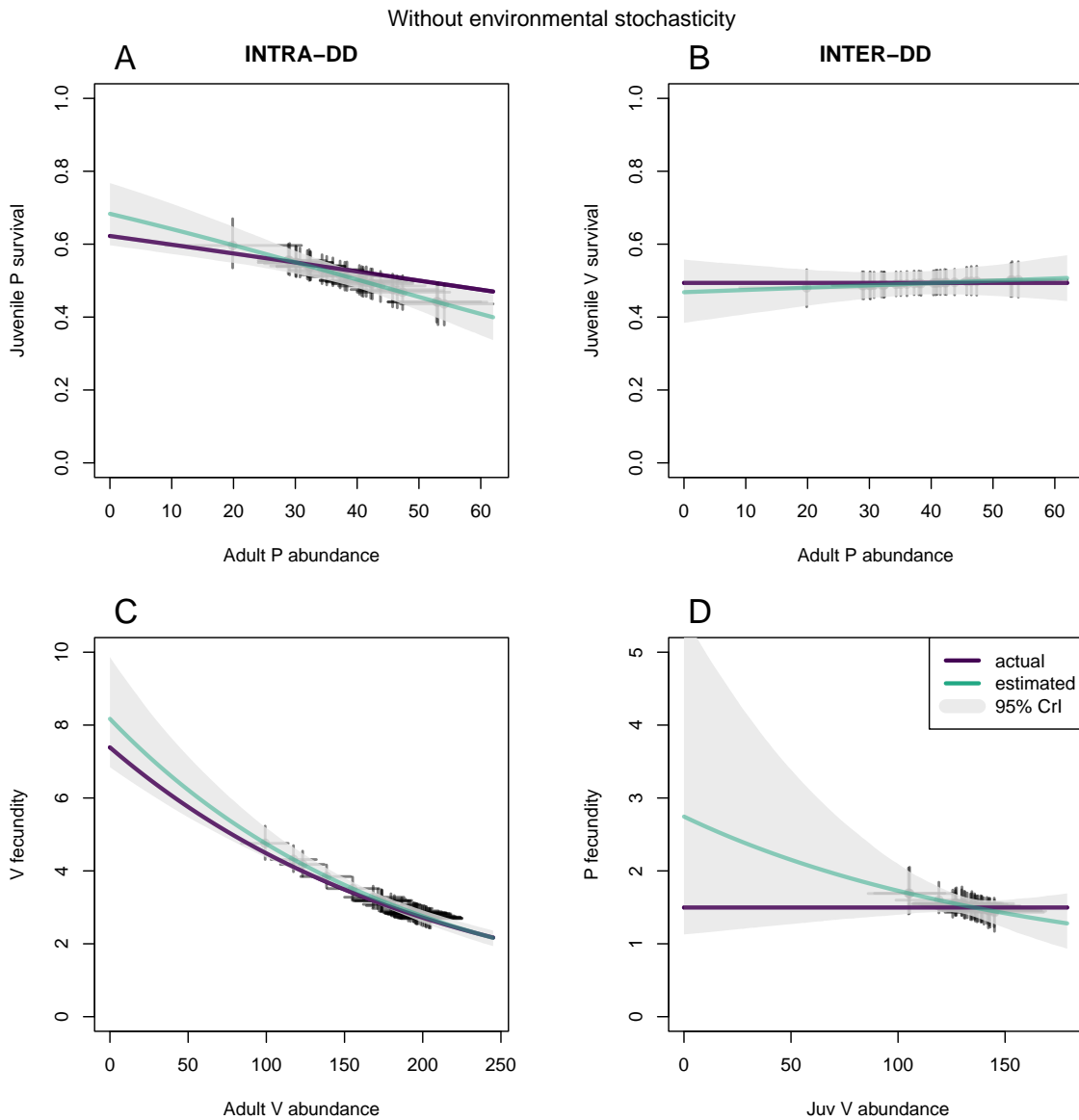


Figure 2: Example of posterior mean (blue-green line) and 95% Credible Intervals (grey polygons) of density-dependencies for juvenile survival rates (**A** for predator and **B** for prey) as well as prey (**C**) and predator (**D**) fecundities estimated by one of the 100 models run in the scenario without random time variation. Purple lines indicate the simulated (true) relationships. Points represent estimated mean demographic parameter each year plotted against estimated yearly abundance values and vertical and horizontal error bars their respective 95% Credible Intervals.

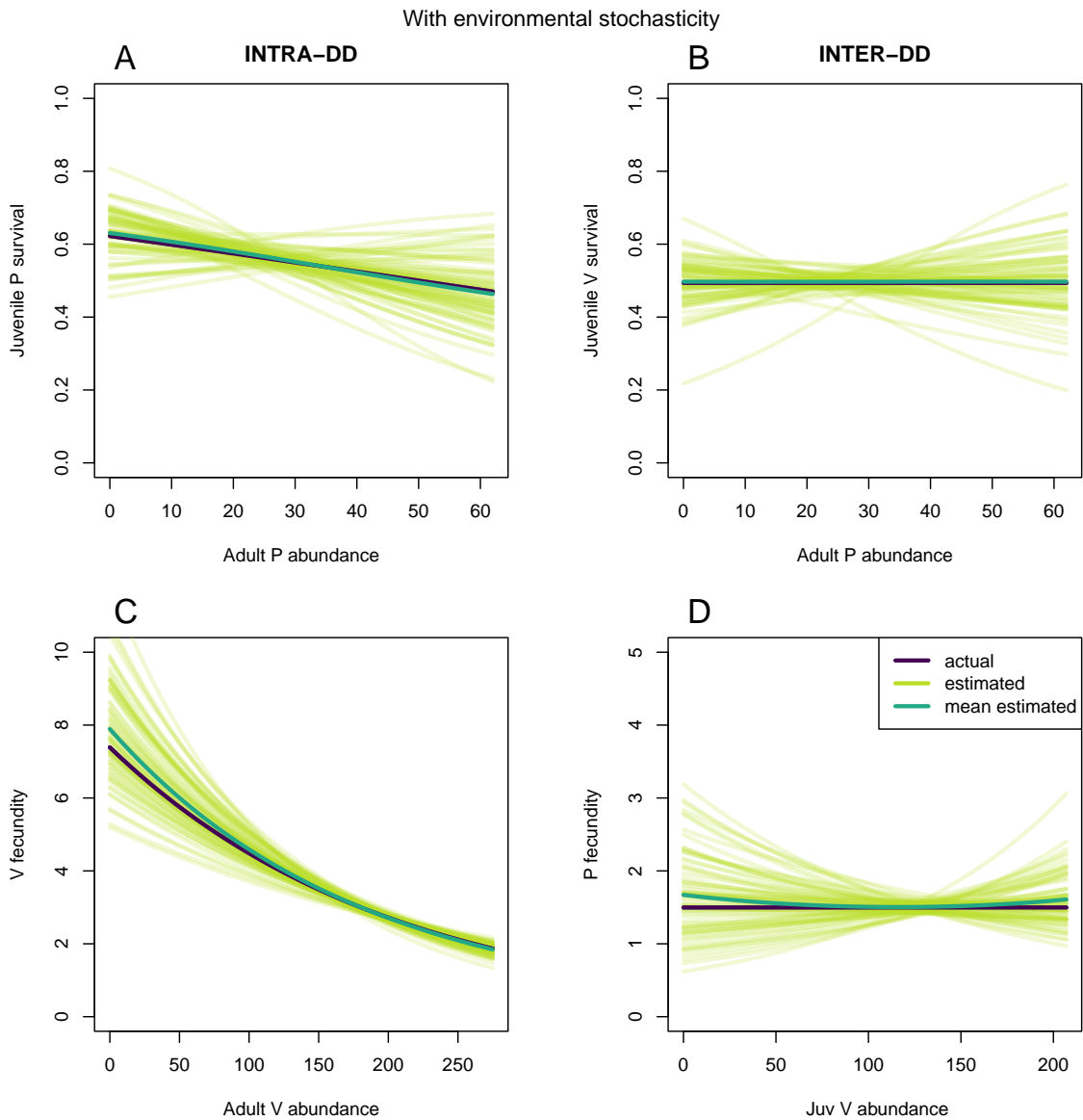


Figure 3: Density-dependencies for juvenile survival rates (**A** for predator and **B** for prey) as well as prey (**C**) and predator (**D**) fecundities in the scenario with random time variation. Purple: simulated relationships, light green: posterior mean relationships for the 73 fitted models that appear to converge satisfactorily, dark green: average of the posterior mean relationships. True inter species density-dependencies (right panels) were set to be absent.

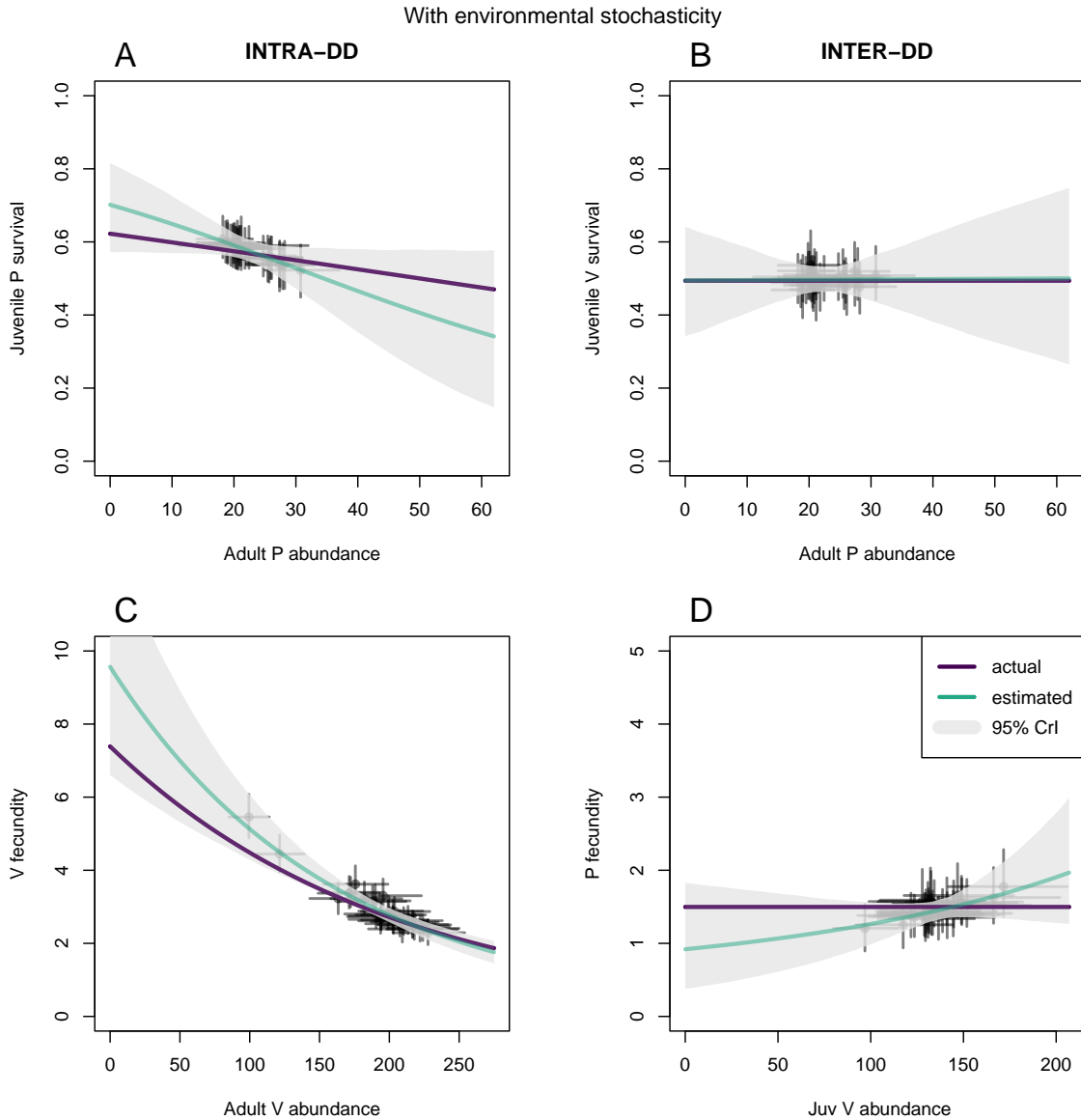


Figure 4: Example of posterior mean (blue-green line) and 95% Credible Intervals (grey polygons) of density-dependencies for juvenile survival rates (**A** for predator and **B** for prey) as well as prey (**C**) and predator (**D**) fecundities estimated by one of the 100 models run in the scenario with random time variation. Purple lines indicate the simulated (true) relationships. Points represent estimated mean demographic parameter each year plotted against estimated yearly abundance values and vertical and horizontal error bars their respective 95% Credible Intervals.

209 We did not detect more false positive species interactions than expected by chance when inves-
 210 tigating the coverage probability of the species interaction parameters at 95% (i.e., the proportion
 211 of simulations where 95% CrI of estimated parameter includes the true parameter value). In the
 212 scenario with 100 juveniles marked each year for 30 years and no interspecific density dependence
 213 nor temporal random variation, this probability was 0.96 for α_4 and 0.94 for α_6 (cf Table 2, see
 214 Figure 2 for an example of estimated mean and pointwise 95% CrI density dependent curves).

215 Coverage probabilities were also satisfactory when interspecific interactions were simulated to be
216 nonzero (0.96 and 0.98). Species interactions parameters were still estimable with no noticeable bias
217 in the presence of random time variation (Figures 3 and 4), in which case the coverage probabilities
218 of the species interaction parameters α_4 and α_6 at 95% were both 0.96 in absence of interspecific
219 interactions (Table 2). In the presence of interspecific interactions, coverage values were similar.
220 Moreover, the addition of random time variation did not noticeably alter the precision of the species
221 interaction parameters, both in absence and presence of species interactions (Figure S3, Table 2).

Table 2: Summary table of parameter estimates. Value refers to the true values used to simulate the data and values of the interspecific density dependent parameters are highlighted in bold. Estimate (95% quantiles) are the mean and the 95% quantiles of the posterior mean estimates. Coverage 95% is the proportion of 95% Credible Intervals that included the true parameter values.

Scenario	Param.	Value	Estimate (95% quantiles)	Coverage 95%
30 years 100 ind. marked/year No temporal noise No interspecies DD	α_1	0.29	0.327 (0.139; 0.585)	0.89
	α_2	-0.01	-0.013 (-0.041; 0.012)	0.89
	α_3	-0.025	-0.033 (-0.197; 0.141)	0.97
	α_4	0	0.001 (-0.015; 0.016)	0.96
	α_5	0.404	0.414 (0.217; 0.601)	0.95
	α_6	0	-0.000 (-0.006; 0.006)	0.94
	α_7	1.24	1.242 (1.194; 1.292)	0.96
	α_8	-0.005	-0.005 (-0.006; -0.004)	0.95
30 years 100 ind. marked/year Temporal noise No interspecies DD	α_1	0.29	0.314 (0.110; 0.527)	0.95
	α_2	-0.01	-0.012 (-0.031; 0.011)	0.96
	α_3	-0.025	-0.013 (-0.209; 0.172)	0.93
	α_4	0	0.000 (-0.018; 0.022)	0.96
	α_5	0.404	0.401 (0.223; 0.561)	0.93
	α_6	0	0.000 (-0.004; 0.006)	0.96
	α_7	1.24	1.246 (1.160; 1.316)	0.92
	α_8	-0.005	-0.005 (-0.007; -0.004)	0.96
30 years 100 ind. marked/year No temporal noise Interspecies DD	α_1	0.29	0.325 (0.179; 0.552)	0.94
	α_2	-0.01	-0.012 (-0.033; 0.002)	0.96
	α_3	-0.025	-0.009 (-0.175; 0.180)	0.95
	α_4	-0.025	-0.026 (-0.043; -0.010)	0.96
	α_5	0.404	0.403 (0.285; 0.556)	0.95
	α_6	0.004	0.004 (-0.002; 0.008)	0.98
	α_7	1.24	1.243 (1.191; 1.296)	0.90
	α_8	-0.005	-0.005 (-0.007; -0.004)	0.92
30 years 100 ind. marked/year Temporal noise Interspecies DD	α_1	0.29	0.334 (0.149; 0.536)	0.97
	α_2	-0.01	-0.015 (-0.029; 0.005)	0.96
	α_3	-0.025	-0.017 (-0.218; 0.174)	0.95
	α_4	-0.025	-0.025 (-0.044; -0.009)	1
	α_5	0.404	0.404 (0.282; 0.537)	0.92
	α_6	0.004	0.004 (-0.001; 0.008)	0.96
	α_7	1.24	1.234 (1.164; 1.311)	0.91
	α_8	-0.005	-0.005 (-0.007; -0.003)	0.88

222 4 Discussion

223 Building on the multispecies integrated predator-prey model of [Barraquand & Gimenez \(2019\)](#), we
224 investigated here whether multispecies IPMs could output interactions where there are in fact none.
225 We did so by modelling functions relating vital rates to stage-specific species densities, whose slope
226 parameters are used to model species interactions. We found that when those slopes were simulated
227 as zero, the estimates were centered on zero and therefore unbiased. There was also a good coverage
228 probability of interaction parameters (close to 0.95 for 95% CrIs). We also found that adding noise to
229 these multispecies density-dependent link functions did not alter these results (although parameter
230 estimation was less often possible in this case, see discussion below). This confirms that multispecies
231 IPMs are a promising way to estimate species interactions, and in particular, that they could be
232 used to infer whether two species interact or not when such information is missing.

233 An important additional outcome of our study pertains to the sample size needed to be able to
234 estimate intra and interspecific interactions, which is likely higher than previously anticipated. By
235 adding observation error on count data ($\sigma_{obs}^2 = 0.1$ on the log scale) to allow for identifiability of
236 stage-specific abundances, we had to increase the sample size of the capture-mark-recapture dataset
237 used in [Barraquand & Gimenez \(2019\)](#) up to 100 prey individuals and 100 predator individuals newly
238 marked every years for 30 years, in order to reach practical identifiability of the density dependence
239 parameters and satisfactory convergence of the MCMC chains for a large majority of the datasets
240 (i.e., 98/100). Estimation was still unbiased with the data designs considered in [Barraquand &](#)
241 [Gimenez \(2019\)](#) but failing for a number of datasets. When adding unexplained environmental
242 stochasticity (i.e., random time variation on the link functions), the proportion of converging MCMC
243 chains went down to 73/100 datasets, which means that density dependence parameters could be
244 satisfactorily estimated for about three quarters of the datasets. These proportions were highly
245 similar when interspecific interactions were present (i.e., 97/100 and 74/100 respectively). This
246 raises the question of how common such large datasets are for (suspected) predator-prey population
247 pairs. That being said, parameter estimation was still possible with smaller sample sizes in many
248 cases (i.e., 44/100 datasets in the worse case studied, [Figure S8](#)), and the only predator-prey IPM
249 using real data so far used 22 years of capture recapture histories for 318 predators and 1210 prey
250 individuals (i.e., c.a. 14 and 55 individuals per year respectively).

251 In field population studies, additional types of data available are likely to improve estimation of
252 species interactions and we give three examples below. First, when age classes can be determined

253 during the count observation process, including such information explicitly in the model (see e.g.,
254 [Weegman *et al.*, 2016](#); [Paquet *et al.*, 2019](#)) will increase identifiability and/or precision of survival
255 parameters and age specific abundances, and therefore will likely improve the estimation of density
256 dependence parameters as well. This stage-specific abundance information may also allow, in some
257 cases where counts are provided with little error, to remove the observation process, which we
258 cannot do in our current model formulation because the observed population size sums adult and
259 juvenile densities, and this sum has to arise from a probability distribution (Equations (2) and (3)).
260 Second, integrating dead recovery data of prey is likely to give extra information on the strength of
261 predator-prey interactions. Dead recoveries are classically implemented in capture-mark-recovery
262 models ([Seber, 1972](#); [North & Morgan, 1979](#)) which in some cases can be combined with CMR
263 data ([Barker, 1999](#)) and counts ([Reynolds *et al.*, 2009](#)). Since the probability to find a dead prey
264 is likely affected by predation rates in the population (e.g., in some systems prey eaten will not be
265 recovered, in others dead recoveries may present signs of predation), taking the predation process
266 into account in the dead recoveries data-generation mechanism could improve the estimation of the
267 strength of predator-prey interactions. Finally, the spatial structure of the data should contain
268 additional information that may help to estimate parameters. The extension to spatially explicit
269 IPMs ([Chandler & Clark, 2014](#); [Zhao, 2020](#)) for interacting populations represents a promising way
270 forward for the estimation of species interactions.

271 Although our results are encouraging, the efficiency of multispecies IPMs in estimating species
272 interactions may also depend on the parameter set, and thus on the ecological features of the
273 populations studied. For example, the parameters considered here correspond well to vertebrate
274 predator-prey systems with a stable equilibrium in absence of environmental perturbations. Faster
275 life histories, different stage or age structure, and multiple factors contributing to altering the
276 quantity of information encapsulated in the various data streams may alter the sample sizes required
277 for efficient inferences. When applying these models to new systems with different life history
278 parameters and density-dependent structures, simulated datasets with plausible ecological features
279 for the empirical system considered (and similar data designs), will help confirm that parameter
280 values can be recovered without bias and with sufficient precision. Tools such as JAGS ([Plummer
281 *et al.*, 2003](#)) or Nimble ([de Valpine *et al.*, 2017](#)) make it particularly handy to both simulate and fit
282 data with complex dynamic models.

283 Acknowledgements

284 We thank Olivier Gimenez for discussion of these analyses and comments on the manuscript.

285 Colleagues from IMB and Biogeco labs are thanked for a welcoming environment.

286 Funding

287 Funding was provided through grant ANR-20-CE45-0004 to FB.

288 References

289 Abadi, F., Gimenez, O., Ullrich, B., Arlettaz, R. & Schaub, M. (2010). Estimation of immigration
290 rate using integrated population models. *Journal of Applied Ecology*, 47, 393–400.

291 Auger-Méthé, M., Field, C., Albertsen, C.M., Derocher, A.E., Lewis, M.A., Jonsen, I.D. &
292 Mills Flemming, J. (2016). State-space models’ dirty little secrets: even simple linear gaussian
293 models can have estimation problems. *Scientific reports*, 6, 1–10.

294 Barker, R.J. (1999). Joint analysis of mark—recapture, resighting and ring-recovery data with
295 age-dependence and marking-effect. *Bird Study*, 46, S82–S91.

296 Barraquand, F. & Gimenez, O. (2019). Integrating multiple data sources to fit matrix population
297 models for interacting species. *Ecological modelling*, 411, 108713.

298 Barraquand, F., Picoche, C., Detto, M. & Hartig, F. (2021). Inferring species interactions using
299 granger causality and convergent cross mapping. *Theoretical Ecology*, 14, 87–105.

300 Besbeas, P., Freeman, S.N., Morgan, B.J. & Catchpole, E.A. (2002). Integrating mark–recapture–
301 recovery and census data to estimate animal abundance and demographic parameters. *Biometrics*,
302 58, 540–547.

303 Brooks, S.P. & Gelman, A. (1998). General methods for monitoring convergence of iterative simu-
304 lations. *Journal of computational and graphical statistics*, 7, 434–455.

305 Burnham, K.P. (1987). *Design and analysis methods for fish survival experiments based on release-
306 recapture*. American Fisheries Society.

307 Chandler, R.B. & Clark, J.D. (2014). Spatially explicit integrated population models. *Methods in*
308 *Ecology and Evolution*, 5, 1351–1360.

309 de Valpine, P., Paciorek, C., Turek, D., Michaud, N., Anderson-Bergman, C., Obermeyer, F.,
310 Wehrhahn Cortes, C., Rodríguez, A., Temple Lang, D., Paganin, S. & Hug, J. (2022). Nimble:
311 Mcmc, particle filtering, and programmable hierarchical modeling.

312 de Valpine, P., Turek, D., Paciorek, C., Anderson-Bergman, C., Temple Lang, D. & Bodik, R.
313 (2017). Programming with models: writing statistical algorithms for general model structures
314 with NIMBLE. *Journal of Computational and Graphical Statistics*, 26, 403–417.

315 Gelman, A. & Rubin, D.B. (1992). Inference from iterative simulation using multiple sequences.
316 *Statistical science*, pp. 457–472.

317 Kéry, M. & Schaub, M. (2011). *Bayesian population analysis using WinBUGS: a hierarchical*
318 *perspective*. Academic Press.

319 Knape, J. (2008). Estimability of density dependence in models of time series data. *Ecology*, 89,
320 2994–3000.

321 Lahoz-Monfort, J.J., Harris, M.P., Wanless, S., Freeman, S.N. & Morgan, B.J. (2017). Bringing it
322 all together: multi-species integrated population modelling of a breeding community. *Journal of*
323 *Agricultural, Biological and Environmental Statistics*, 22, 140–160.

324 McElreath, R. (2020). *Statistical rethinking: A Bayesian course with examples in R and Stan*.
325 Chapman and Hall/CRC.

326 North, P.M. & Morgan, B.J. (1979). Modelling heron survival using weather data. *Biometrics*, pp.
327 667–681.

328 Paquet, M., Arlt, D., Knape, J., Low, M., Forslund, P. & Pärt, T. (2019). Quantifying the links
329 between land use and population growth rate in a declining farmland bird. *Ecology and evolution*,
330 9, 868–879.

331 Péron, G. & Koons, D.N. (2012). Integrated modeling of communities: parasitism, competition,
332 and demographic synchrony in sympatric ducks. *Ecology*, 93, 2456–2464.

333 Plummer, M., Best, N., Cowles, K. & Vines, K. (2006). Coda: Convergence diagnosis and output
334 analysis for mcmc. *R News*, 6, 7–11.

335 Plummer, M. *et al.* (2003). Jags: A program for analysis of bayesian graphical models using gibbs
336 sampling. In: *Proceedings of the 3rd international workshop on distributed statistical computing*.
337 Vienna, Austria., vol. 124, pp. 1–10.

338 Ponisio, L.C., de Valpine, P., Michaud, N. & Turek, D. (2020). One size does not fit all: Customizing
339 mcmc methods for hierarchical models using nimble. *Ecology and evolution*, 10, 2385–2416.

340 Qu erou e, M., Barbraud, C., Barraquand, F., Turek, D., Delord, K., Pacoureau, N. & Gimenez,
341 O. (2021). Multispecies integrated population model reveals bottom-up dynamics in a seabird
342 predator–prey system. *Ecological monographs*, 91, e01459.

343 R Core Team (2022). *R: A Language and Environment for Statistical Computing*. R Foundation
344 for Statistical Computing, Vienna, Austria.

345 Reynolds, T.J., King, R., Harwood, J., Frederiksen, M., Harris, M.P. & Wanless, S. (2009). In-
346 tegrated data analysis in the presence of emigration and mark loss. *Journal of Agricultural,*
347 *Biological, and Environmental Statistics*, 14, 411–431.

348 Sander, E.L., Wootton, J.T. & Allesina, S. (2017). Ecological network inference from long-term
349 presence-absence data. *Scientific reports*, 7, 1–12.

350 Seber, G. (1972). Estimating survival rates from bird-band returns. *The Journal of Wildlife Man-*
351 *agement*, pp. 405–413.

352 Strydom, T., Catchen, M.D., Banville, F., Caron, D., Dansereau, G., Desjardins-Proulx, P., Forero-
353 Mu noz, N.R., Higino, G., Mercier, B., Gonzalez, A. *et al.* (2021). A roadmap towards predicting
354 species interaction networks (across space and time). *Philosophical Transactions of the Royal*
355 *Society B*, 376, 20210063.

356 Tibbits, M.M., Groendyke, C., Haran, M. & Liechty, J.C. (2014). Automated factor slice sampling.
357 *Journal of Computational and Graphical Statistics*, 23, 543–563.

358 Weegman, M.D., Bearhop, S., Fox, A.D., Hilton, G.M., Walsh, A.J., McDonald, J.L. & Hodgson,
359 D.J. (2016). Integrated population modelling reveals a perceived source to be a cryptic sink.
360 *Journal of Animal Ecology*, 85, 467–475.

361 Zhao, Q. (2020). On the sampling design of spatially explicit integrated population models. *Methods*
362 *in Ecology and Evolution*, 11, 1207–1220.

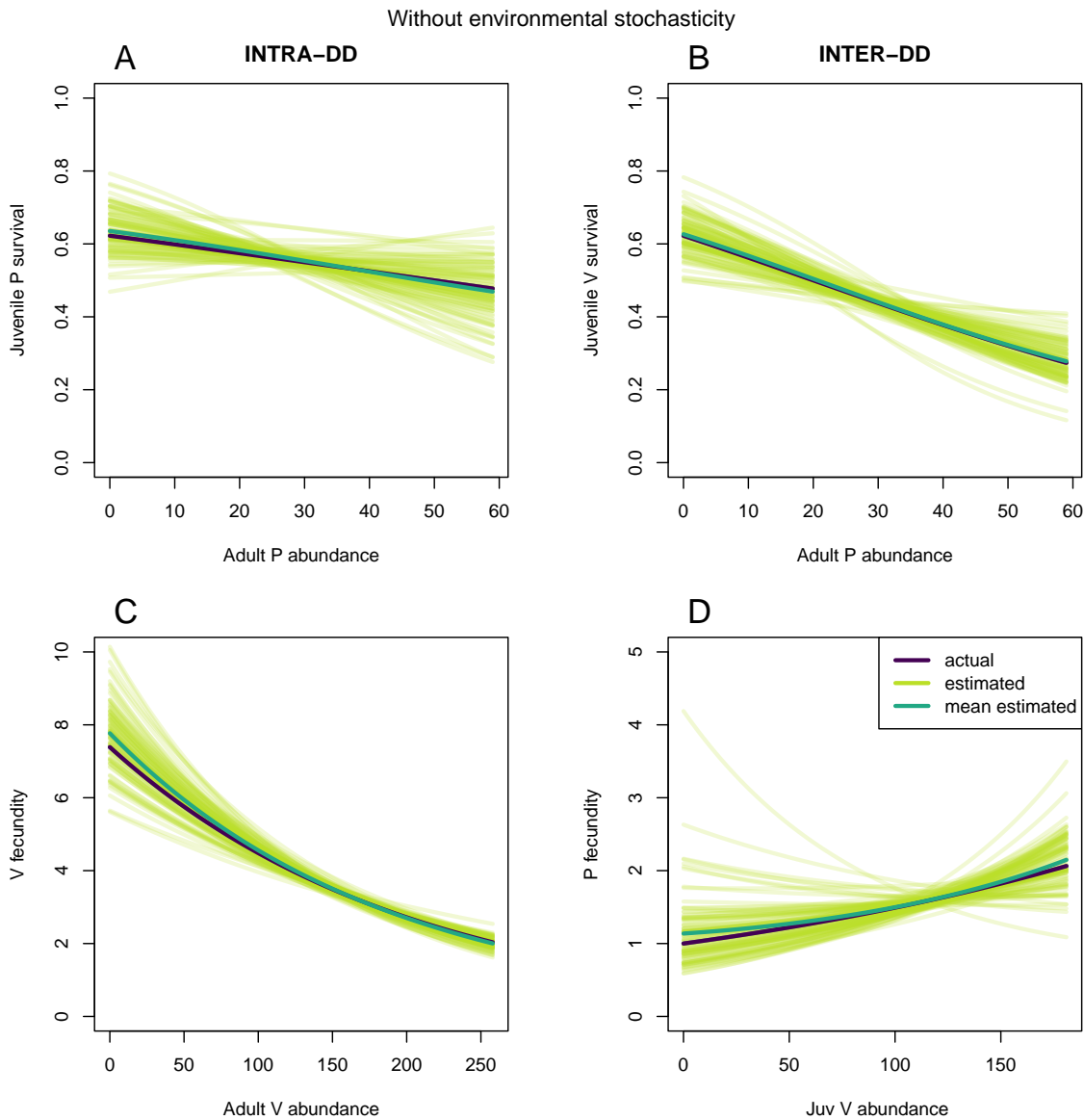
364 **A Results from the scenarios in presence of species interactions**

Figure S1: Density-dependencies for juvenile survival rates (**A** for predator and **B** for prey) as well as prey (**C**) and predator (**D**) fecundities in the scenario without random time variation in presence of true inter species density-dependencies. Purple: simulated relationships, light green: posterior mean relationships for the 97 fitted models that appear to converge satisfactorily, dark green: average of the posterior mean relationships.

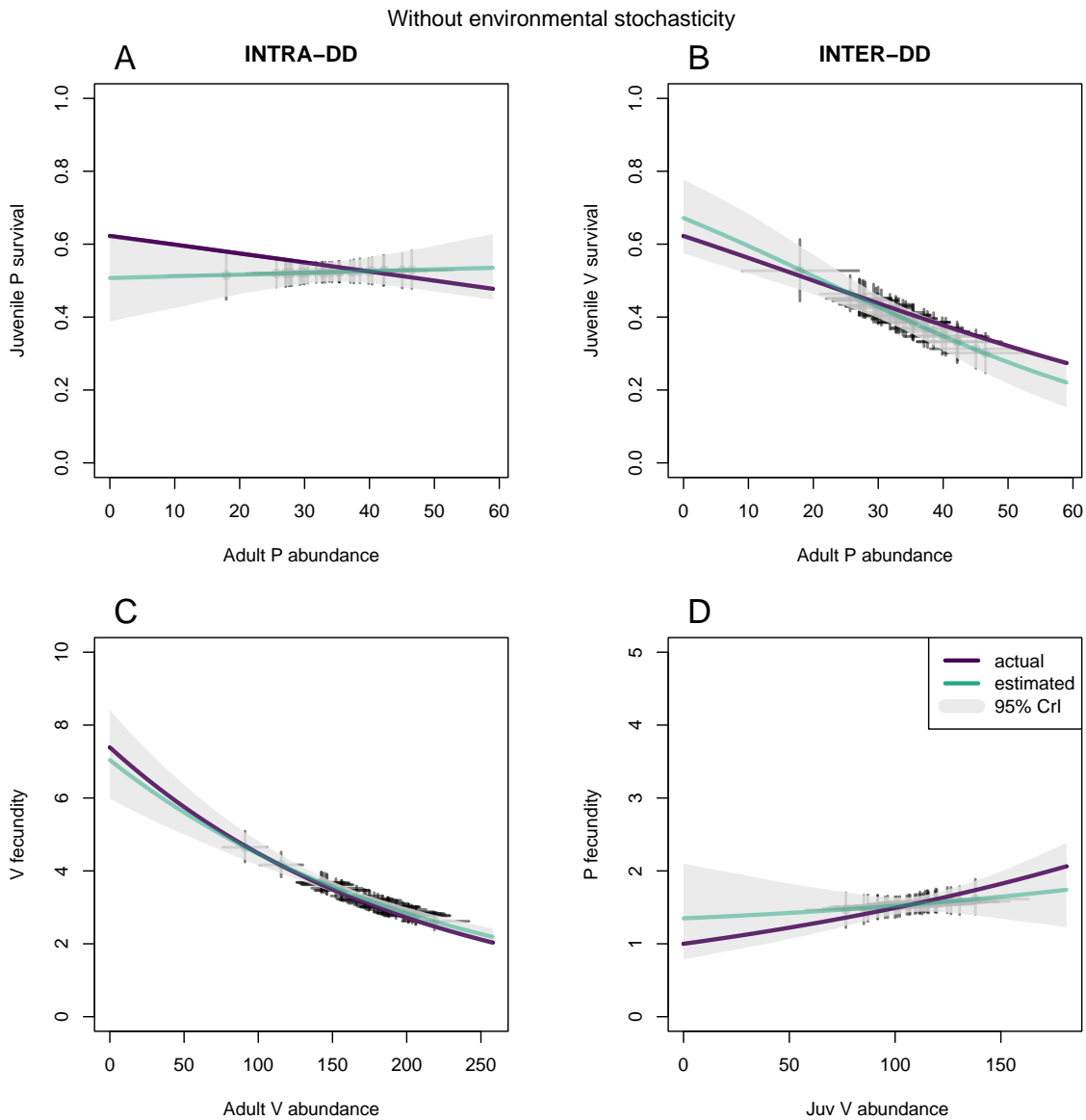


Figure S2: Example of posterior mean (blue-green line) and 95% Credible Intervals (grey polygons) of density-dependencies for juvenile survival rates (**A** for predator and **B** for prey) as well as prey (**C**) and predator (**D**) fecundities estimated by one of the 100 models run in the scenario without random time variation in presence of true inter species density-dependencies. Purple lines indicate the simulated (true) relationships. Points represent estimated mean demographic parameter each year plotted against estimated yearly abundance values and vertical and horizontal error bars their respective 95% Credible Intervals.

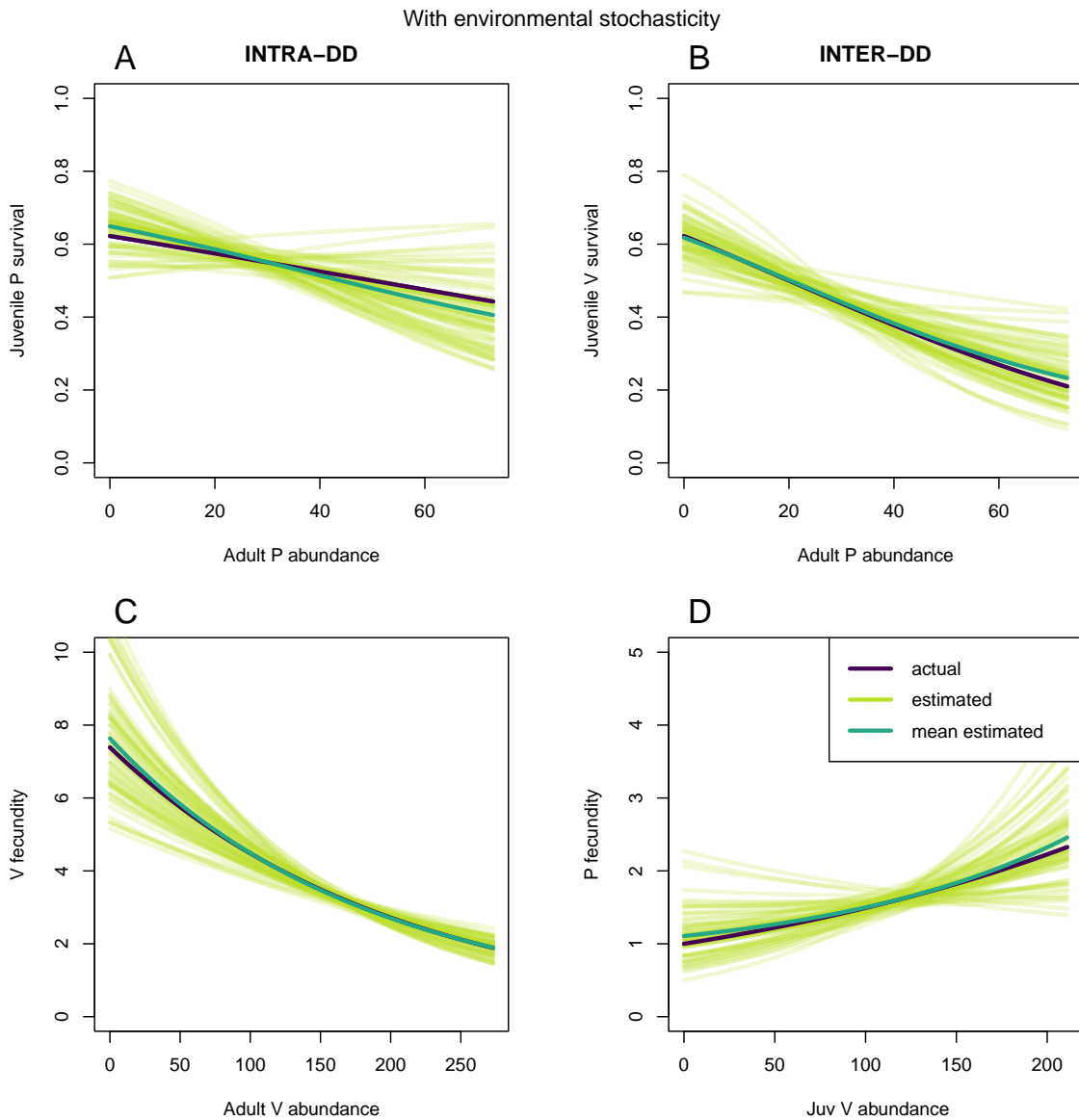


Figure S3: Density-dependencies for juvenile survival rates (**A** for predator and **B** for prey) as well as prey (**C**) and predator (**D**) fecundities in the scenario with random time variation in presence of true inter species density-dependencies. Purple: simulated relationships, light green: posterior mean relationships for the 74 fitted models that appear to converge satisfactorily, dark green: average of the posterior mean relationships.

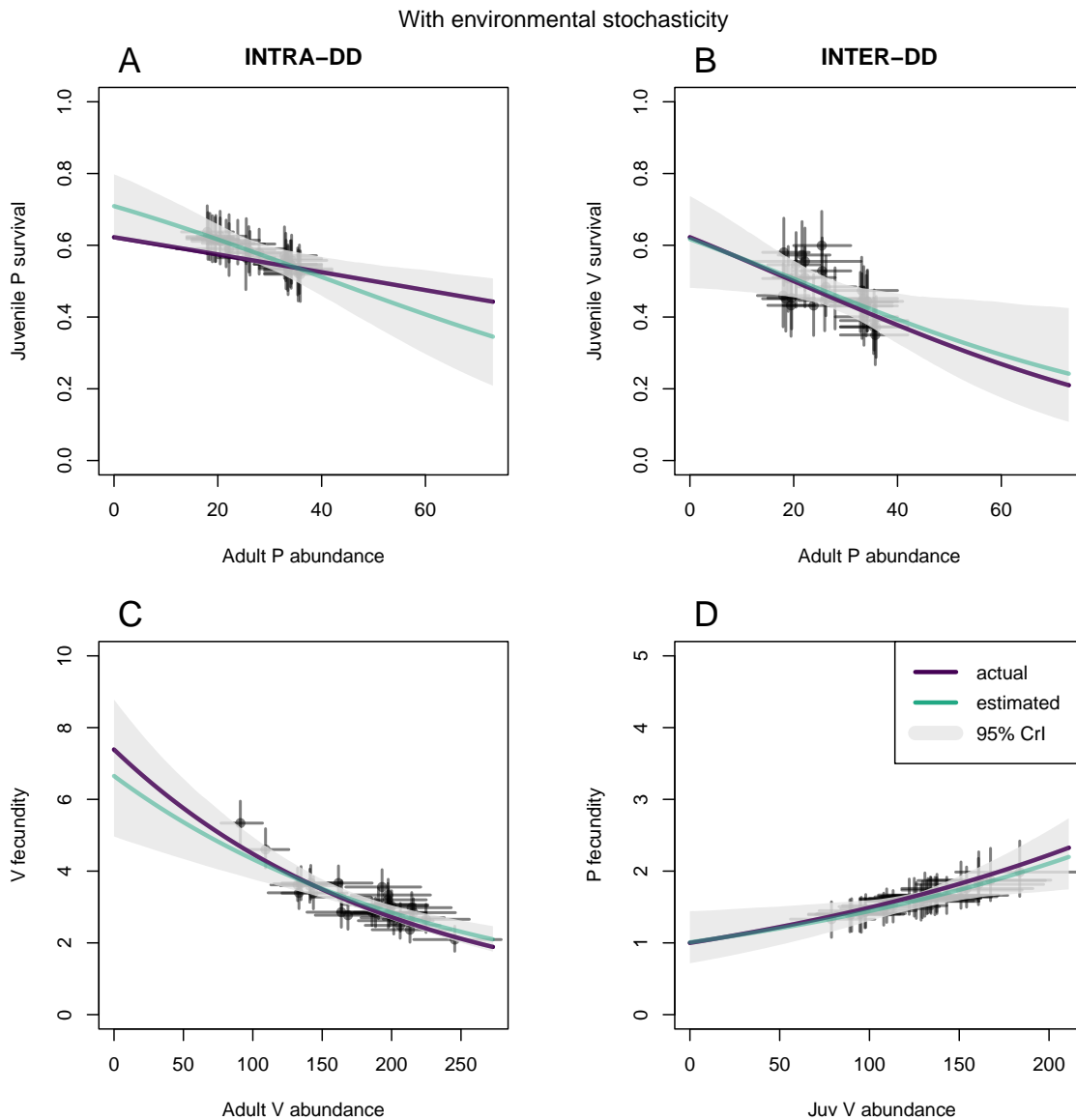


Figure S4: Example of posterior mean (blue-green line) and 95% Credible Intervals (grey polygons) of density-dependencies for juvenile survival rates (**A** for predator and **B** for prey) as well as prey (**C**) and predator (**D**) fecundities estimated by one of the 100 models run in the scenario with random time variation in presence of true inter species density-dependencies. Purple lines indicate the simulated (true) relationships. Points represent estimated mean demographic parameter each year plotted against estimated yearly abundance values and vertical and horizontal error bars their respective 95% Credible Intervals.

365 **B Results from the scenarios with 100 juveniles of each species marked each year**
366 **for 10 years, and 20 juveniles of each species marked for 30 years, without**
367 **centering abundances in the link functions**

Table S1: Value refers to the true values used to simulate the data and values of the interspecific density dependent parameters are highlighted in bold. Estimate (95% quantiles) are the mean and the 95% quantiles of the posterior mean estimates. Coverage 95% is the proportion of 95% Credible Intervals that included the true parameter values.

Scenario	Param.	Value	Estimate (95% quantiles)	Coverage 95%
10 years 100 ind. marked/year No temporal noise	α_1	0.50	0.506 (-0.136; 1.422)	0.97
	α_2	-0.01	-0.003 (-0.051; 0.018)	0.97
	α_3	-0.025	0.043 (-0.608; 0.684)	0.98
	α_4	0	-0.003 (-0.029; 0.023)	0.98
	α_5	0.404	0.304 (-0.491; 1.029)	0.95
	α_6	0	0.001 (-0.004; 0.007)	0.93
	α_7	2	1.995 (1.793; 2.204)	0.98
	α_8	-0.005	-0.005 (-0.007; -0.004)	0.98
10 years 100 ind. marked/year Temporal noise	α_1	0.5	0.287 (-0.178; 0.856)	1
	α_2	-0.01	0.039 (-0.020; 0.488)	0.98
	α_3	-0.025	0.014 (-0.477; 0.615)	1
	α_4	0	-0.001 (-0.027; 0.020)	1
	α_5	0.404	0.330 (-0.208; 0.863)	1
	α_6	0	0.001 (-0.004; 0.005)	1
	α_7	2	1.958 (1.549; 2.293)	0.91
	α_8	-0.005	-0.005 (-0.007; -0.003)	0.93
30 years 20 ind. marked/year No temporal noise	α_1	0.5	0.636 (0.051; 1.366)	0.94
	α_2	-0.01	-0.002 (-0.047; 0.032)	0.97
	α_3	-0.025	0.038 (-0.524; 0.483)	1
	α_4	0	-0.001 (-0.021; 0.018)	0.99
	α_5	0.404	0.312 (-0.502; 1.010)	0.92
	α_6	0	0.001 (-0.004; 0.007)	0.96
	α_7	2	2.00 (1.011; 2.194)	0.94
	α_8	-0.005	-0.005 (-0.006; -0.004)	96
30 years 20 ind. marked/year Temporal noise	α_1	0.5	0.577 (-0.008; 1.161)	0.98
	α_2	-0.01	-0.015 (-0.043; 0.014)	1
	α_3	-0.025	-0.005 (-0.520; 0.363)	0.98
	α_4	0	-0.000 (-0.013; 0.016)	1
	α_5	0.404	0.336 (-0.466; 0.770)	0.98
	α_6	0	0.000 (-0.003; 0.006)	0.98
	α_7	2	1.975 (1.704; 2.264)	0.95
	α_8	-0.005	-0.005 (-0.007; -0.003)	0.95

10 years, without environmental stochasticity

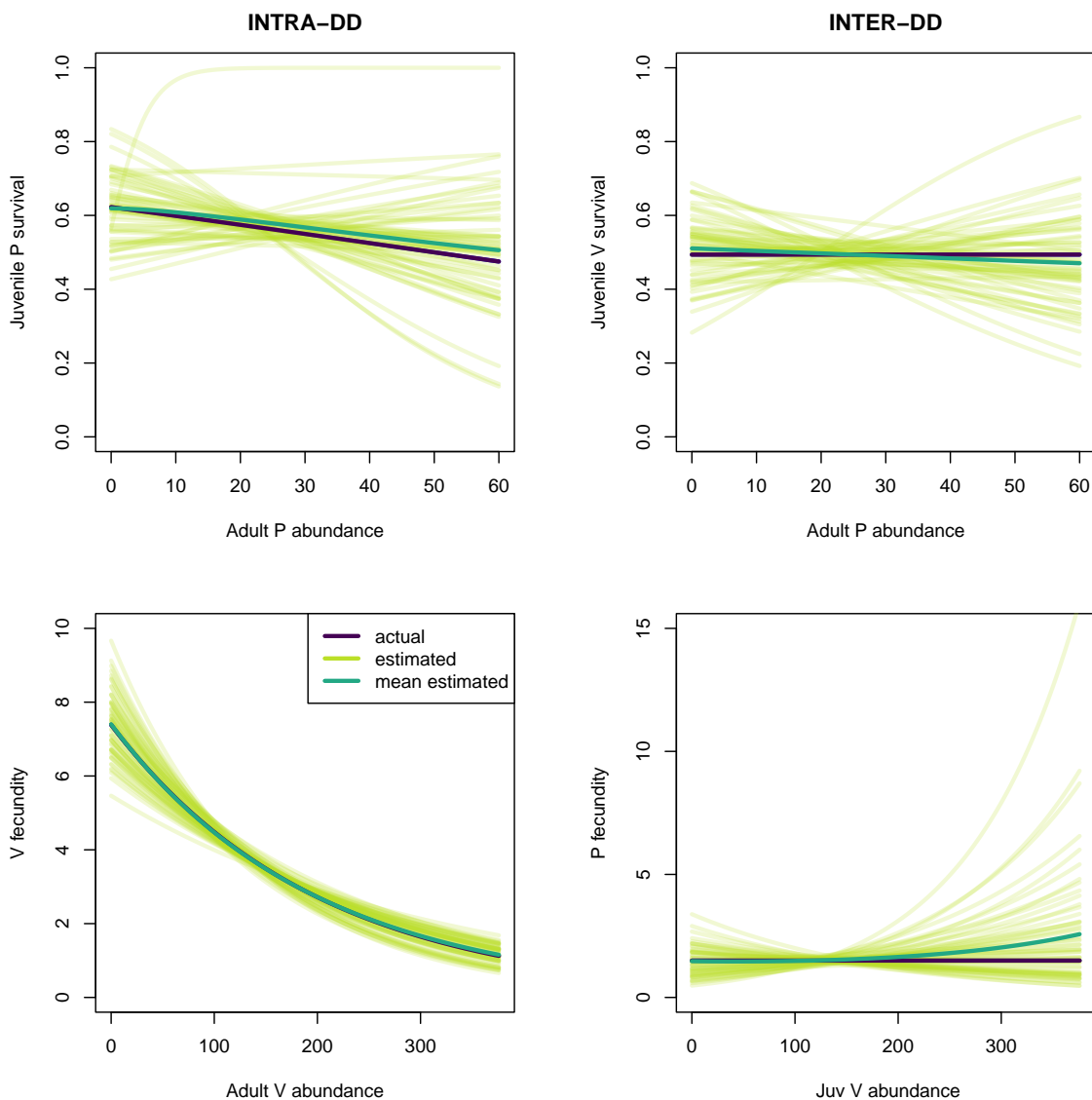


Figure S5: Density-dependencies for juvenile survival rates (**A** for predator and **B** for prey) as well as prey (**C**) and predator (**D**) fecundities in the scenario with 100 juveniles per species marked each year for 10 years without random time variation in absence of true inter species density-dependencies. Purple: simulated relationships, light green: posterior mean relationships for the 59 fitted models that appear to converge satisfactorily, dark green: average of the posterior mean relationships.

10 years, with environmental stochasticity

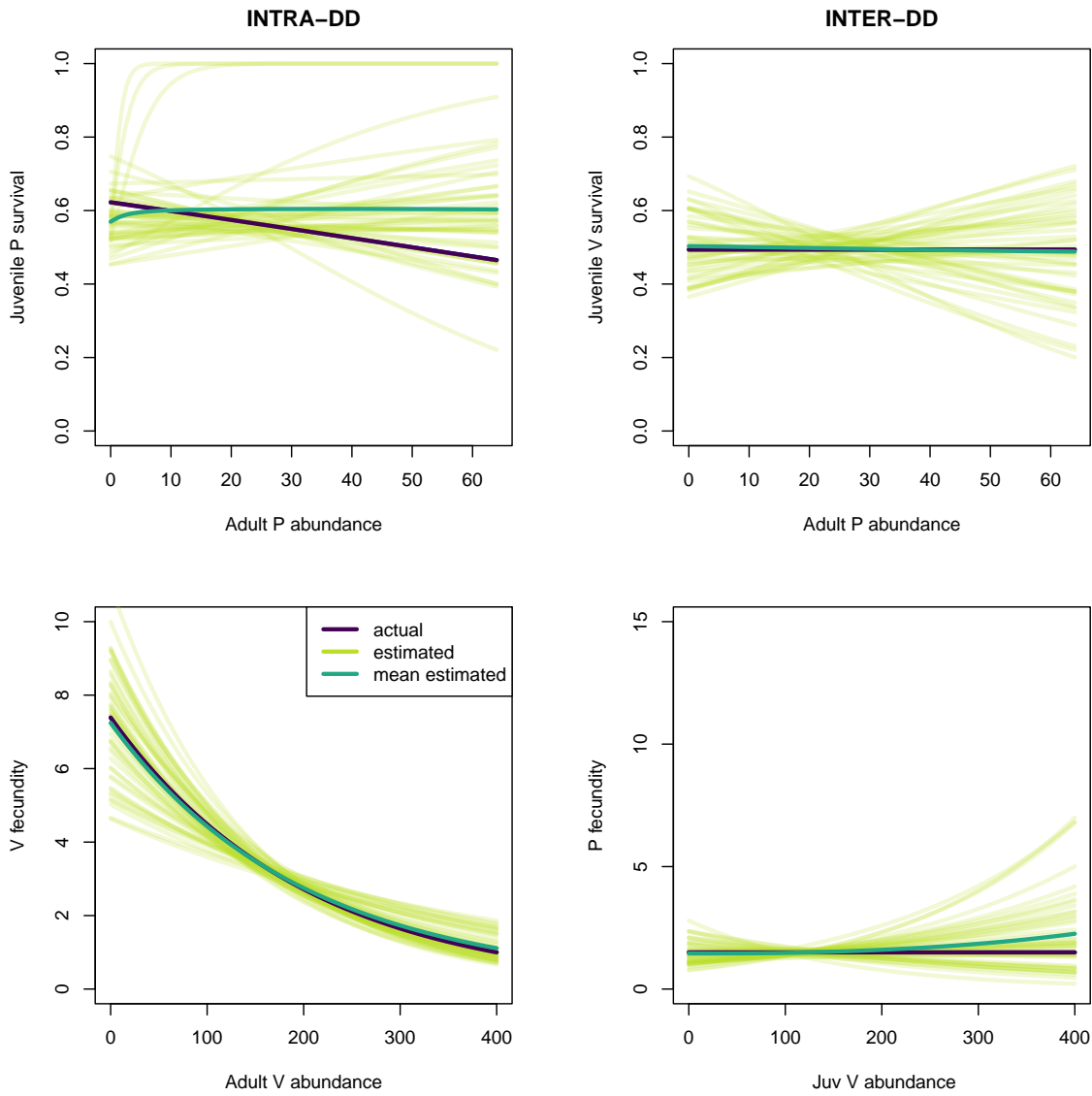


Figure S6: Density-dependencies for juvenile survival rates (**A** for predator and **B** for prey) as well as prey (**C**) and predator (**D**) fecundities in the scenario with 100 juveniles per species marked each year for 10 years with random time variation in absence of true inter species density-dependencies. Purple: simulated relationships, light green: posterior mean relationships for the 46 fitted models that appear to converge satisfactorily, dark green: average of the posterior mean relationships.

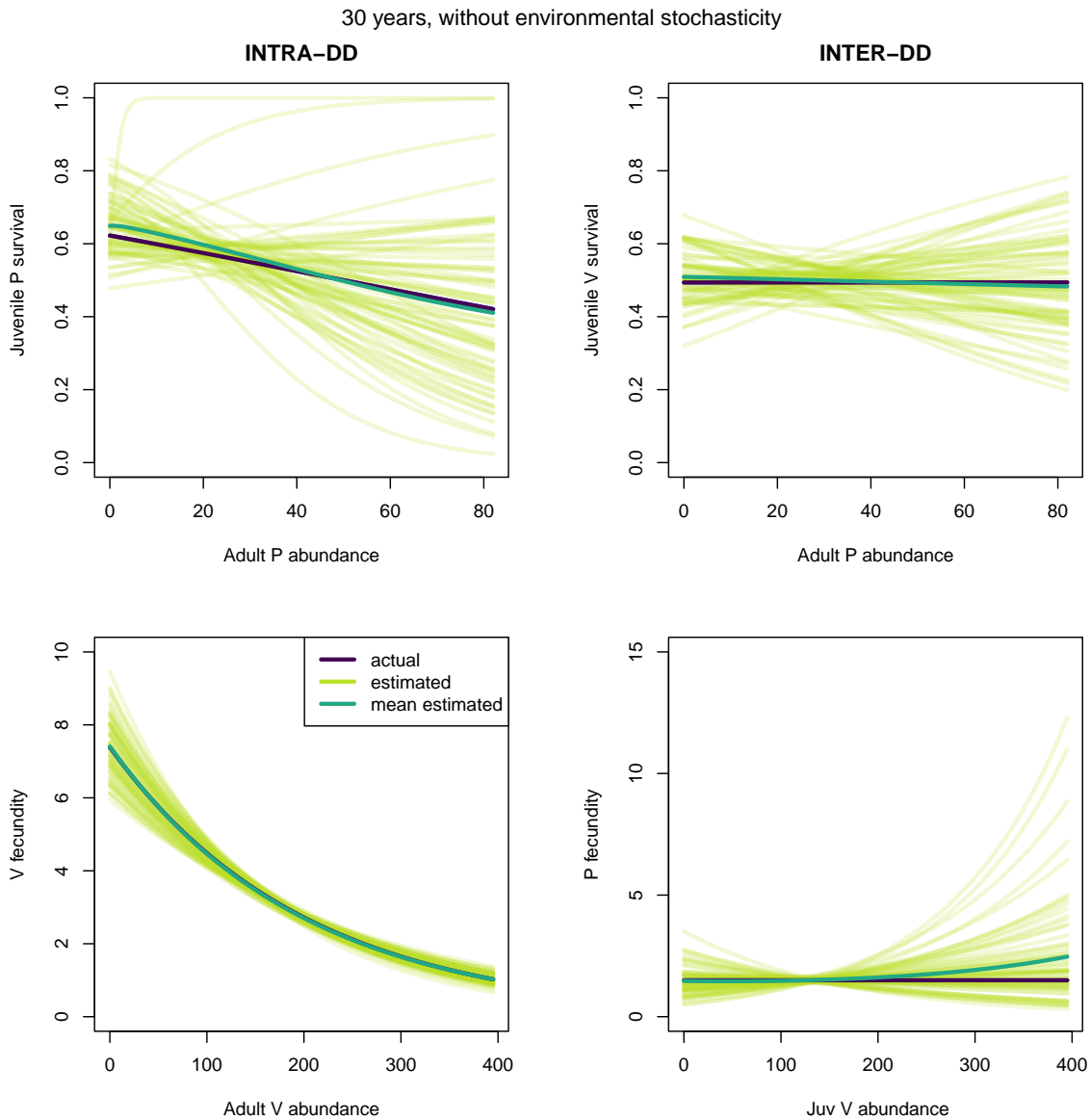


Figure S7: Density-dependencies for juvenile survival rates (**A** for predator and **B** for prey) as well as prey (**C**) and predator (**D**) fecundities in the scenario with 20 juveniles per species marked each year for 30 years without random time variation in absence of true inter species density-dependencies. Purple: simulated relationships, light green: posterior mean relationships for the 71 fitted models that appear to converge satisfactorily, dark green: average of the posterior mean relationships.

30 years, with environmental stochasticity

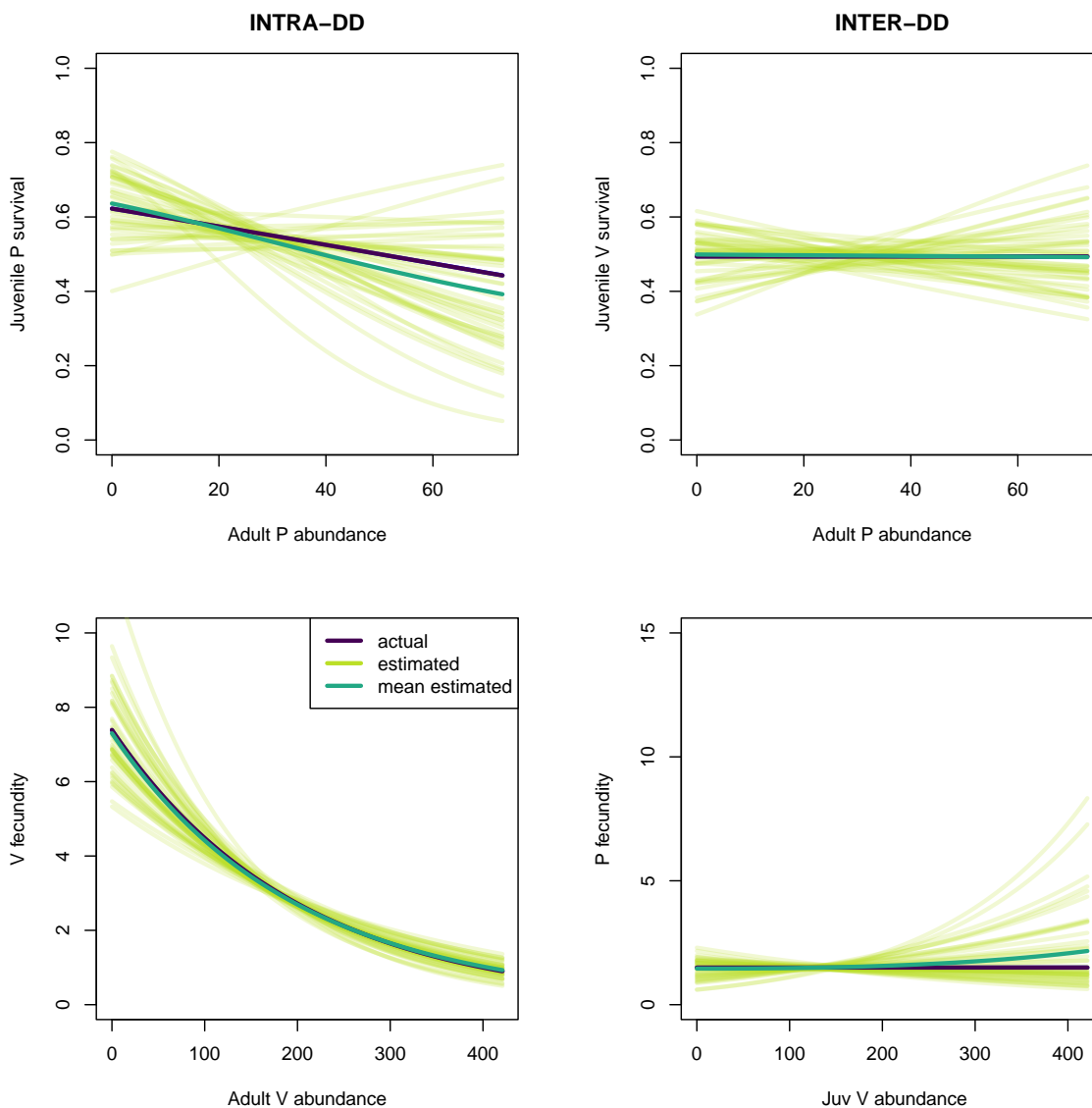


Figure S8: Density-dependencies for juvenile survival rates (**A** for predator and **B** for prey) as well as prey (**C**) and predator (**D**) fecundities in the scenario with 20 juveniles per species marked each year for 30 years with random time variation in absence of true inter species density-dependencies. Purple: simulated relationships, light green: posterior mean relationships for the 44 fitted models that appear to converge satisfactorily, dark green: average of the posterior mean relationships.

368 C Sensitivity of parameter estimation to the choice of initial values

369 To assess whether the accuracy of the estimation of density dependent parameters was condi-
370 tioned by the fact that we used true parameter values as initial values, we also ran the MCMC
371 using values that substantially deviated from the true value and expected posterior distributions.
372 For this study, we used data (and the corresponding model) without temporal random noise and
373 without true interspecific interactions. We chose one simulated dataset for which the true values
374 of α_2 , α_4 , α_6 and α_8 fell well within the 95% credible intervals of the posterior samples when
375 using the true value as initial value (see script [https://github.com/MatthieuPaquet/multi-](https://github.com/MatthieuPaquet/multi-species/blob/main/script_initial_values.R)
376 [species/blob/main/script_initial_values.R](https://github.com/MatthieuPaquet/multi-species/blob/main/script_initial_values.R) for more details on the procedure). We then
377 simulated 100 sets of initial values that deviated from the true values by 4 standard deviations
378 estimated from the posterior samples when the true values were used as initial values (hereafter
379 $SD_{\hat{\alpha}_i}$). For the parameters for which negative density dependence was expected, we simulated
380 the 100 initial values as $\alpha_i^{init} \sim \mathcal{N}(\alpha_i - 4SD_{\hat{\alpha}_i}, SD_{\hat{\alpha}_i})$ whereas for α_8 , which was a potentially
381 positive prey \rightarrow predator link (and would have been assumed positive in an empirical analysis),
382 we used $\alpha_8^{init} \sim \mathcal{N}(\alpha_8 + 4SD_{\hat{\alpha}_8}, SD_{\hat{\alpha}_8})$. We used true parameter values as initial values for all
383 other model parameters. Preliminary runs showed that convergence was reached very quickly
384 (typically after a couple of iterations) with efficient mixing. We then ran 2 chains for 1200 it-
385 erations and discarded the first 200 as burn-in and did not use thinning. For comparison we
386 also run 2 MCMC chains once, under the same settings, using the true values as initial val-
387 ues (see script [https://github.com/MatthieuPaquet/multi-species/blob/main/script_MCMC-](https://github.com/MatthieuPaquet/multi-species/blob/main/script_MCMC_simulated_initial_values_out_of_posterior.R)
388 [simulated_initial_values_out_of_posterior.R](https://github.com/MatthieuPaquet/multi-species/blob/main/script_MCMC_simulated_initial_values_out_of_posterior.R)). The results showed no sign of influence of the
389 initial value chosen on the parameter estimates (Figure S9).

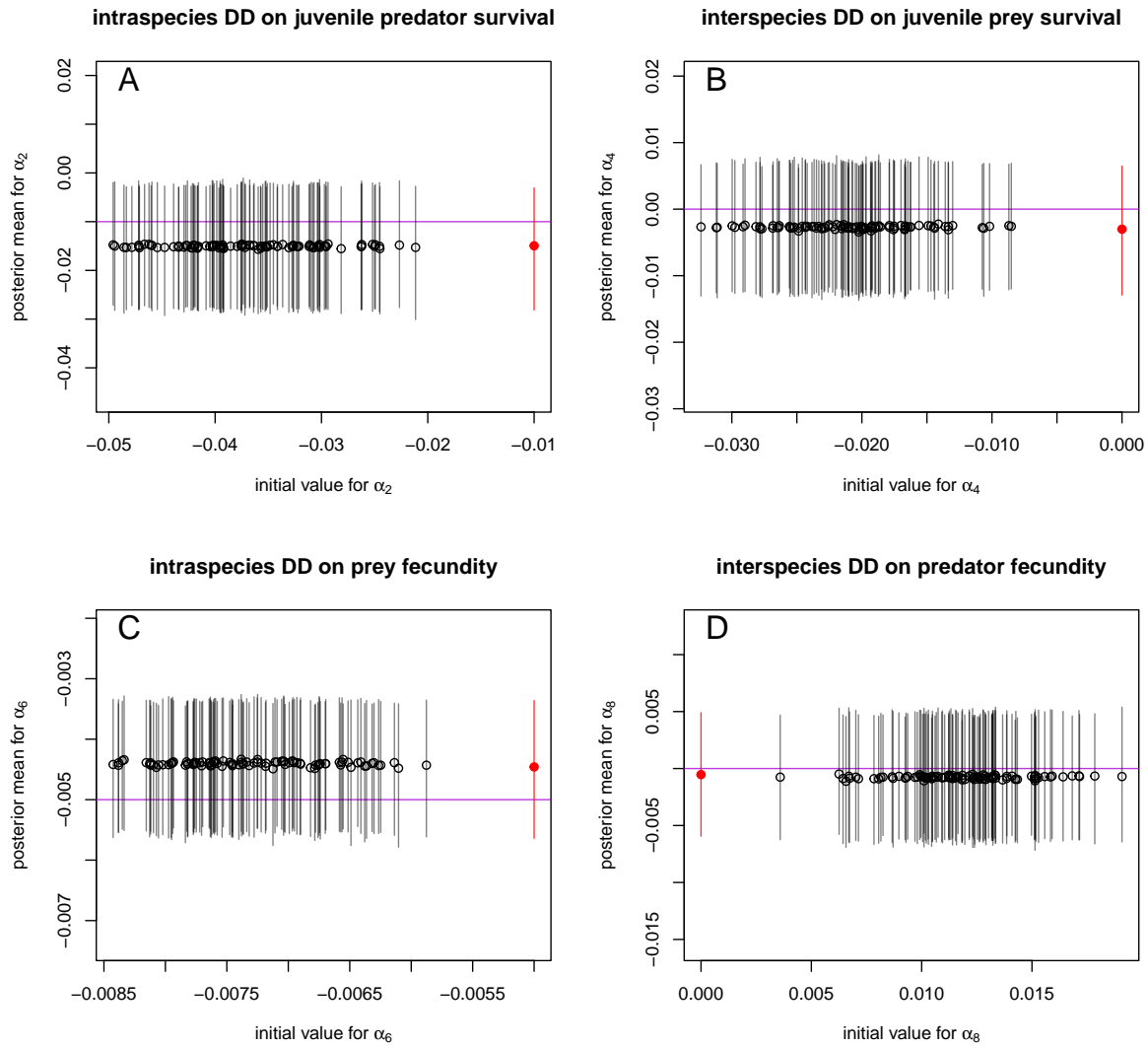


Figure S9: Estimation of density dependent parameter values (α_2 in panel **A**, α_4 in panel **B**, α_6 in panel **C** and α_8 in panel **D**) in relation to the initial values chosen to start the MCMC chains. Dots show the posterior means and vertical lines the 95% credible intervals. Purple horizontal lines highlight the value used to simulate the data. Red dots and intervals show the case where the true values are used as initial values.